Charge migration through DNA molecules in the presence of mismatches

M. H. Lee, S. Avdoshenko, R. Gutierrez, and G. Cuniberti
Institute for Materials Science and Max Bergmann Center of Biomaterials, Dresden University of Technology, D-01062 Dresden, Germany

(Received 16 June 2010; revised manuscript received 6 August 2010; published 28 October 2010)

Charge transport characteristics of short double-strand DNA including mismatches are studied within a methodology combining molecular-dynamics (MD) simulations and electronic-structure calculations based on a fragment orbital approach. Electronic parameters and transmission probabilities are computed along the MD trajectory. We find that in the course of the MD simulation the energetic position of frontier orbitals may be interchanged. As a result, the highest-occupied molecular orbital can temporarily have a large weight on the backbones as a function of time. This shows that care must be taken when projecting the electronic structure onto effective low-dimensional model Hamiltonians to calculate transport properties. Further, the transport calculations indicate a suppression of the charge migration efficiency when introducing a single GT or AC mismatch in the DNA sequence.

DOI: 10.1103/PhysRevB.82.155455 PACS number(s): 73.63.−b, 87.14.gk, 81.07.Pr, 82.20.Wt

I. INTRODUCTION

The charge-transfer phenomenology of DNA has attracted considerable attention in recent years due to the practical consequences they may have in the development of electronic devices based on molecular assemblies[1] or, more recently, for the purpose of DNA sequencing.[2,3] Experimental measurements[4–10] on the electric conduction properties of DNA attached to metal electrodes have shown many different results so far: insulating,[4–7] semiconductorlike,[8] and metalliclike.[9,10] In particular, transport experiments performed on double-strand (ds) DNA molecules covalently attached to metal electrodes showed similar high currents for different base sequences and DNA lengths. For example, Cohen *et al.*[9] measured a 220 nA current at 2 V bias for 26-base pair dsDNA, and Xu *et al.*[10] obtained a conductance of 0.1 μS for poly$(GC)_8$. In both experiments the dsDNA molecules were connected to gold electrodes via an S-Au bond. Similarly, Kang *et al.*[11] found currents on the order of 100 nA at 2 V using mechanically controllable break junctions for an inhomogeneous sequence of 30 base pairs dsDNA. The relatively broad spectrum of experimental predictions hints at the complex interplay of many factors determining the charge migration efficiency through DNA segments. They include, among others, the environment, the coupling between the molecule and the external world (electrodes), dynamical disorder rising from the strong fluctuations in the DNA atomic frame but also mediated by environmental fluctuations, and the specific base sequence. This situation makes the reproducibility of DNA charge transport experiments very difficult as well as a theoretical analysis, see Refs. 12–14 for recent reviews. While there is agreement that long DNA sequences are insulating, the situation is not so clear concerning shorter oligomers with up to 30 base pairs.

Carbon nanotube (CNT)-DNA molecular junctions[15] have been considered as an attractive option to obtain reproducible electrical conductivity measurements of DNA oligomers; moreover the low dimensionality of CNT as well as its chirality-dependent electronic structure opens the possibility to tune the electrical response of the junction. Recently, Guo *et al.*[16] have investigated the influence of point mismatches on the conductance of a 15-base pair DNA molecule connected to CNT electrodes via amide linkages. It was found that a single GT or CA mismatch in a DNA 15-mer increases the resistance of the DNA by a factor of roughly ~300 compared to a well-matched one. The effect of base pair mismatches on the conductance has been also studied by Hihath *et al.*[17] for 11- and 12-base pairs dsDNA chemically bound to gold electrodes via thiol linkers. The experiments showed a change in the conductance of dsDNA by as much as an order of magnitude depending on the type of mismatches. These results suggest the possibility of detecting a mutation in dsDNA by measuring the change in the electrical conductance of the molecule[18] and it thus opens fascinating options for the development of biosensors based on modifications of the electrical response.

Many efforts[19–35] have been performed to analyze charge propagation through DNA oligomers from both the theoretical and the experimental points of view. Although for hole transfer in solutions there seems to be some agreement that the hole motion takes place in an incoherent manner, the microscopic charge transport mechanisms for DNA contacted by electrodes still seem to remain elusive, since a purely incoherent hopping mechanism does not seem to be able to yield electrical currents in the order of nanoampere as observed in some experiments.[9–11,16] However, an important result emerging from several studies[20,22,24,26] is that dynamical effects play a fundamental role and cannot in general be treated as a small perturbation to an otherwise static structure. Hence, their inclusion in charge transport calculations is crucial, which makes necessary the comparison of different approaches dealing with dynamical effects on different approximation levels.

Motivated by the above-mentioned experiments,[9–11,16] and especially by the results of Ref. 16, we investigate in this paper charge transport in dsDNA oligomers with a well-matched base pair sequence and with two types of single mismatched base pairs (AT→GT, GC→AC) in the presence of solvent and counterions. A schematic representation is shown in Fig. 1. We consider metallic electrodes consisting of (5,5) carbon nanotubes with the dsDNA molecule being

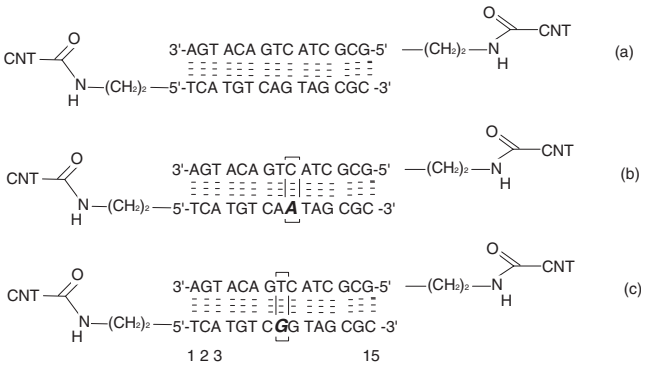

FIG. 1. Schematic of dsDNA with (a) well-matched sequence, (b) a single mismatch of AC at the site 9, and (c) a single mismatch of GT at the site 8. The dsDNA is covalently bonded to (5,5) metallic CNT via amide linker.

covalently bonded to the CNT via amide linkages on both ends. To take into account the effect of dynamical fluctuations on the charge-transfer parameters, we combine classical molecular-dynamics (MD) with quantum-mechanical (QM) electronic-structure calculations along the classical MD trajectory using the hybrid QM/MM (quantum mechanics/molecular mechanics) method[36,37] in the presence of solvent and counterions. The electronic parameters obtained from this hybrid methodology provide an input for the formulation of low-dimensional effective model Hamiltonians[24–26] which can in their turn be used for charge transport calculations. We discuss two possible alternatives of coarse graining the electronic structure based on different ways of estimating the most relevant electronic states for transport. In Sec. II we explain in some detail our methodology to obtain the electronic-structure parameters for charge transfer and define the model Hamiltonian for charge-transport calculations. A discussion of the charge-transfer parameters and the time-averaged transmission functions is finally presented in Sec. III. Lastly, we summarize our conclusions in Sec. IV.

II. METHODOLOGY

A. Molecular-dynamics simulation

Classical MD simulations were performed using the Amber99 force field with the AMBER10 package.[38] The 15-mer dsDNA connected to the (5,5) CNT via amide linker was solvated with transferable intermolecular potentials within the three-site water model (TIP3P) (Ref. 39) water molecules in a rectangular box of $70\times70\times120$ Å^3. Counterions ($28Na^+$) were added to neutralize the system. The total number of atoms in the system is thus $\sim7\times10^4$. The system was equilibrated for about 500 ps at 300 K after a heating procedure from 0 to 300 K. The MD simulations were performed at 300 K using an *NVT* thermostat with a time step of 0.5 fs and periodic boundary conditions. Snapshots along the MD trajectory were drawn every 1 fs out of a total simulation time of 1 ps.

B. Electronic-structure calculation

The electronic-structure calculations for dsDNA were performed using a fragment orbital approach[40–43] to efficiently perform a coarse graining of the molecular electronic structure with inclusion of the environmental effects. In our approach a fragment consists of a pair of nucleotides (phosphate-deoxyribose-nucleobase) from each DNA strand. Time-dependent charge-transfer parameters—on-site energies $\varepsilon_i(t)$ of fragment i and transfer integrals $T_{i,j}(t)$ between fragments—were calculated for each snapshot along the MD trajectory. The electronic couplings $T_{i,j}(t)$ are computed only between the nearest-neighbor fragments ($j=i\pm1$) and only one relevant molecular orbital (MO) from each fragment (ψ_i,ψ_j) is considered. We stress, however, that this is only done for the sake of simplification; our methodology is flexible enough to include a larger Hilbert space into the transport calculations. The transfer integrals can be expressed as $T_{i,j}=\langle\psi_i|H|\psi_j\rangle$. By expanding the molecular-orbital basis in terms of valence atomic orbitals η_μ, $\psi_i=\Sigma_\mu c_\mu^i\eta_\mu$, we obtain

$$T_{ij}=\sum_{\mu\nu}c_\mu^i c_\nu^j\langle\eta_\mu|H|\eta_\nu\rangle=\sum_{\mu\nu}c_\mu^i c_\nu^j H_{\mu\nu}. \quad (1)$$

The fragment orbital approach has been widely used to obtain charge-transfer parameters in DNA.[24–26] In most cases, however, a base pair is chosen as a fragment and the highest-occupied MO (HOMO) of the fragment is used as ψ_i and ψ_j. In our case, we choose a nucleotide as the building block of a fragment. In the next section we will show that level crossing effects due to the dynamics of the system makes such a choice the most natural one. The electronic-structure calculations to obtain $H_{\mu\nu}$ and c_μ are performed using a hybrid QM/MM scheme[36,37] implemented in the AMBER10 package. Each fragment (nucleotide pair) is considered as a QM region and the remaining part of the system including solvent and counterions belongs to the MM region. In this way we can take into account the effect of solvent and counterions on the charge-transfer parameters. The semiempirical Hamiltonian AM1 (Ref. 44) was used for the QM calculations. Along the MD trajectory QM/MM calculations are performed for each fragment to generate the coefficients c_μ^i and for two adjacent fragments to produce the Hamiltonian matrix elements $H_{\mu\nu}$.

At this point we are going to introduce two possible selection criteria which allow us to further coarse grain the multilevel electronic structure. This will make it possible to map the electronic system onto a simpler tight-binding model with linear topology and with a single orbital per site while identifying semiquantitatively relevant pathways for charge migration:

(1) *Criterion I.* The relevant pair (between nearest neighbors) of fragment molecular orbitals at a given time is chosen in such a way that $|T_{i,j}|$ is maximized subject to an upper cutoff for the energy difference between neighboring fragment on-site energies: $\Delta\varepsilon_{i,i+1}=|\varepsilon_i-\varepsilon_{i+1}|<\Delta\varepsilon_0$. This maximizes the electronic coupling while not allowing the energetic barriers between the two effective sites to exceed a certain maximum threshold. We computed $T_{i,j}$ for a range of molecular orbitals (HOMO, … ,HOMO-15) while imposing the condition that $\Delta\varepsilon_0\sim1.5$ eV. The choice of the threshold to lie around 1.5 eV was guided by the well-known statistical 3σ criterion, where σ is the variance of the probability distribution of the onsite energies. We considered the threshold

value to be around $3-4\sigma$. Additional tests with higher values of $\Delta\varepsilon_0$ showed that the electronic couplings remained approximately unchanged.

(2) *Criterion II*. The relevant site energies and electronic coupling elements between two fragments are determined out of the full electronic manifold according to the criterion that the quantity $P_{i,i+1}=4T_{i,i+1}^2/[(\Delta\varepsilon_{i,i+1})^2+4T_{i,i+1}^2]$ is maximized. Clearly, this option will not provide a maximized electronic coupling along the chain since the site-to-site energy gap is also allowed to vary to yield the maximal $P_{i,i+1}$. This quantity can be seen as a sort of effective tunneling parameter, e.g., when the gap between two given levels vanishes, $P_{i,i+1}$ becomes 1, a behavior which resembles the limiting value of the transmission function for a dimer model when evaluated at the resonance energies (eigenvalues of the dimer Hamiltonian). We remark that molecular orbitals heavily localized onto the backbones and with a strong σ character were excluded from the selection process since they are not expected to contribute to charge-transfer processes.

C. Charge transport and time-average transmission function

Once the effective model Hamiltonian for the electronic structure of the DNA oligomers has been built up, it can be extended to include the coupling to left (L) and right (R) electrodes in order to deal with the charge-transport problem,

$$H=\sum_i \varepsilon_i(t)d_i^\dagger d_i+\sum_i T_{i,i+1}(t)(d_i^\dagger d_{i+1}+\text{H.c.})+\sum_{\mathbf{k}\in \mathrm{L}} t_{\mathbf{k},\mathrm{L}}(a_{\mathbf{k}}^\dagger d_1+\text{H.c.})+\sum_{\mathbf{k}\in \mathrm{R}} t_{\mathbf{k},\mathrm{R}}(a_{\mathbf{k}}^\dagger d_N+\text{H.c.})+\sum_{\mathbf{k}\in \mathrm{L,R}} \varepsilon_{\mathbf{k}}a_{\mathbf{k}}^\dagger a_{\mathbf{k}}. \quad (2)$$

In the previous expression we have used the fact that the model is a linear chain, where only the atoms 1 and N couple to the L and R electrodes, respectively. On a first level of approximation we will treat charge transport within the Landauer theory and take into account the influence of structural fluctuations encoded in the time-dependent electronic parameters by calculating at each time step t the quantum-mechanical transmission function $T(E,t)$ and performing afterward a time average.[24–26] This approach assumes that the time scale of the charge propagation (which is not specified by the MD simulation) is the shortest one. The transmission function $T(E,t)$ can then be written as

$$T(E,t)=4\Gamma_{\mathrm{L}}\Gamma_{\mathrm{R}}|G_{1N}(E,t)|^2, \quad (3)$$

where Γ_{L} and Γ_{R} are effective coupling terms to the L and R leads, respectively. We are using the wide-band approximation, replacing the energy-dependent coupling terms by constants. In the following we chose $\Gamma_{\mathrm{L}}=\Gamma_{\mathrm{R}}\sim 100$ meV. $G_{1N}(E)$ is the 1, N-matrix element of the chain Green's function, which can be calculated via the matrix Dyson's equation,

$$\mathbf{G}^{-1}(E,t)=E\mathbf{1}-\mathbf{H}(t)-\Sigma_{\mathrm{L}}-\Sigma_{\mathrm{R}},$$

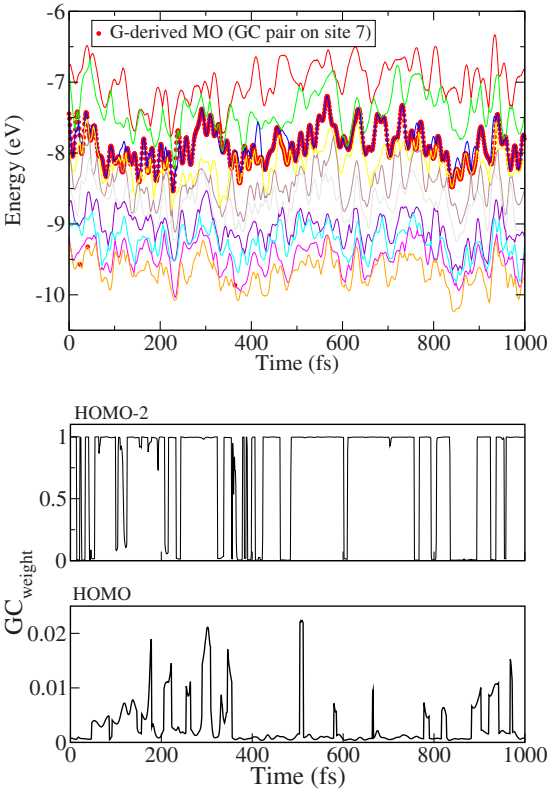

FIG. 2. (Color online) Upper panel: molecular-orbital energy levels for a selected site (7:GC) for a matched dsDNA along a 1 ps MD trajectory (only the occupied states are shown from the HOMO level). The molecular orbitals most strongly localized onto the guanine nucleobase are shown as circles; they lie below the HOMO level (mostly being the HOMO-2 level). Lower panel: time evolution of the GC weight (charge density) for two selected fragment orbitals HOMO-2 and HOMO on the (7:GC) position. Notice the low weight that the HOMO is carrying, indicating that this orbital is not mainly related to the bases, but has rather a large weight on the DNA backbone.

$$(\Sigma_{\mathrm{L}})_{lj}=-i\Gamma_{\mathrm{L}}\delta_{l1}\delta_{j1}, \quad (\Sigma_{\mathrm{R}})_{lj}=-i\Gamma_{\mathrm{R}}\delta_{lN}\delta_{jN}. \quad (4)$$

Note that the time dependence in the previous expression is only a parametric one: the transport properties are calculated at each time step and a time average is performed. We stress that our goal is to highlight the average influence of dynamical fluctuations onto the charge transport. This approach will provide an estimate for the order of magnitude of the coherent component of the charge propagation in a dynamically disordered potential landscape.

III. RESULTS AND DISCUSSION

A. Characteristics of the effective electronic parameters

In this section we first discuss in some detail how the MOs ψ_i, ψ_j required to obtain the relevant electronic parameters are selected. Figure 2 shows the MO energy levels as a function of the simulation time for the occupied states for site number 7 (corresponding to a GC pair) along the dsDNA in a well matched sequence [see also Fig. 1(a) for reference—in what follows we shorten the notation to 7:GC].

The MO energies fluctuate significantly along the MD trajectory due to the interaction with the environment.[29] Notice that the MO energy level from the guanine (G) nucleobase, highlighted by circles, appears a few levels below the HOMO level. The HOMO and (HOMO-1) MOs appear to be mainly localized on the backbone and the deoxyribose regions. Since the hole in DNA is expected to be localized onto the purine nucleobases (A,G) due to their lower ionization potential, this result indicates that within the used electronic-structure methodology the relevant orbitals to be considered to obtain the charge-transfer parameters are not the HOMO but rather orbitals lying deeper in energy. This is further illustrated in the lower panel of Fig. 2, where we show the GC weight as a function of the simulation time for the HOMO and HOMO-2 orbitals of the same fragment. The GC weight is defined as the restricted sum $\Sigma_{\mu\in \mathrm{GC}}|c_\mu^i|^2$ over the eigenvector expansion coefficients c_μ^i of the ith molecular orbital of a fragment. The sum runs only over indices of atomic orbitals centered on the nucleobases. As it becomes clear in Fig. 2 (bottom panel), the HOMO-2 orbital has a large GC weight (on average close to 1) over the simulation time while the HOMO state has a considerably lower contribution from the bases. The oscillatory behavior of the HOMO-2 level clearly suggests that at certain times the GC weight is almost suppressed and the charge density of this orbital is shifted away from the bases. In other words, choosing nucleotide pairs as fragments rather than nucleobases reveals that the character of the molecular orbitals strongly changes from σ-like DNA backbone orbitals to base-localized π orbitals in the course of the MD simulation. This nontrivial behavior suggests that care is needed when defining the appropriate molecular fragment to formulate coarse-grained models dealing with charge transport in biomolecules.

To test the reliability of this result, we have performed additional calculations at a higher level of theory for two different cases: a homogeneous $(GC)_4$ sequence and the sequences in Fig. 1. For the latter, only the innermost eight nucleotide pairs were considered to reduce the computational costs. In both cases a short time (100 fs) MD trajectory was generated by treating the whole dsDNA sequence quantum mechanically using density-functional theory (DFT) with the PADE (LDA with Teter and Pade parametrization) functional[45] and a triple-zeta valence basis with two sets of polarized d functions (TZV2P) atomic basis set as implemented in the CP2K code.[46]

For the two above-mentioned cases we still found the molecular orbital switching between different atomic subsets (backbones and nucleobases) along the MD trajectory. However, the degree of localization (weight) of the HOMO orbital onto the backbones is strongly reduced on the DFT level of theory as compared with the semiempirical AM1 Hamiltonian, i.e., the HOMO level remains localized on the nucleobases over longer time intervals. We remark that the orbital switching behavior can also very much depend on the base sequence so that separate studies must be performed on each specific sequence. For instance, it turns out that the HOMO is localized onto the nucleobases more frequently for a GC fragment than for AT or GT fragments (figure not shown). Recently, it has been found out that the HOMO orbital is localized onto nucleobases, e.g., for $dTMP^-$ (2′-deoxythymidine 5′-monophosphate anion) in vacuum at the CASPT2 level[47] and for a guanine:cytosine dodecamer in the Z conformation in the presence of water and counterions using the DFT Car-Parrinello calculation.[48] We point out that our results concerning the degree of HOMO localization onto the backbone region do not necessarily contradict the previous results since they can sensitively depend on (i) the fact that we compute the electronic structure for geometries along a classical MD trajectory and (ii) on the theory level used to calculate the electronic parameters (semiempirical AM1).[49] We also remark, that when the averaged structure of dsDNA hexamer sequence from MD calculations was used in the presence of water and counterions at the DFT level, it was found that the projected density of states onto the phosphorous atoms has a strong spectral weight just below the Fermi level.[50]

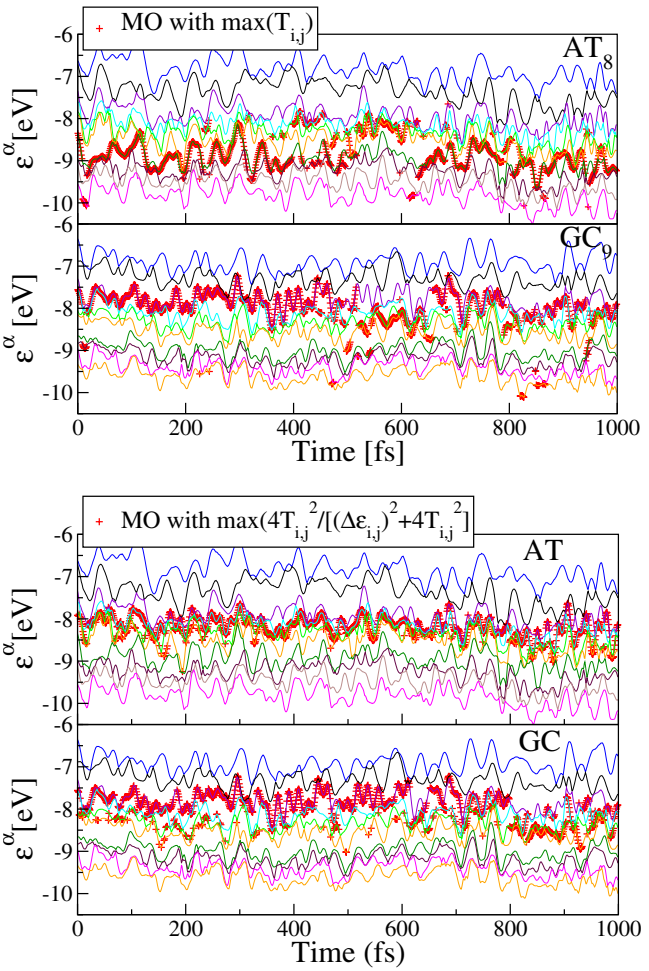

FIG. 3. (Color online) Molecular-orbital energy levels for the two fragments (8:AT and 9:GC) along the 1 ps MD trajectory and for the two different selection criteria I and II introduced in the text. The selected molecular orbitals, according to the criteria I and II, are represented by red(+)symbols for both fragments.

The MO energies, E^*, obtained according to the selection criteria I and II for the neighboring fragments of AT and GC (site 8 and 9) are shown in Fig. 3 [depicted as red(+)symbols]. Notice that for all cases E^* lies energetically

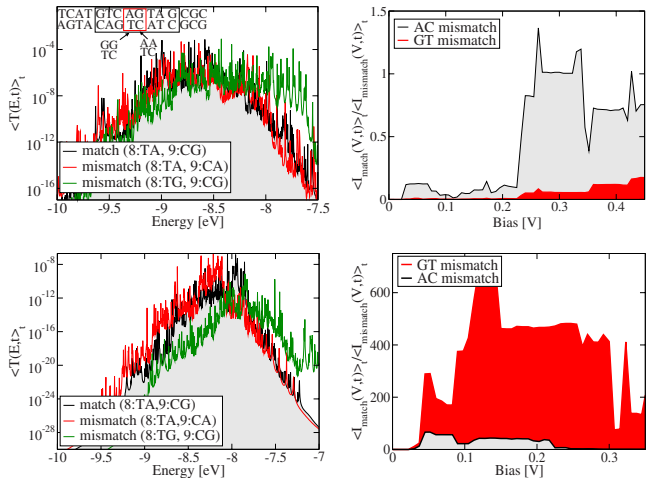

FIG. 4. (Color online) [(a) and (c)] Time-averaged transmissions and [(b) and (d)] corresponding current ratios for criteria I and II and for the three different dsDNA sequences discussed in this study. While for criterion I the main effect of the mismatch is a huge energy shift of the transmission spectrum, especially for GT mismatch, without considerable suppression of transmission, criterion II leads to a very strong reduction in the averaged transmission for GT mismatch. The values of the averaged transmission are in general also smaller in case II than in case I. Notice the strong current suppression for both mismatched sequences when using criterion II.

well below the HOMO level. Each selected E^* exhibits its distinct characteristics as well. For criterion I, E^* appears at a lower energy for an AT fragment compared to E^* by criterion II, which results in a larger energy gap between neighboring fragments. This is because the relevant MOs in case I are chosen only to maximize the transfer integral regardless of the on-site energy alignment. On the other hand, the on-site energies between neighboring fragments are more effectively aligned for criterion II.

B. Charge-transport properties

In Fig. 4 the time averaged transmissions as a function of the injection energy are shown for the criteria I and II. As we can see, criterion I gives a larger average transmission for both matched and mismatched sequences when compared with criterion II. The main effect of introducing a mismatch for criterion I turns out to be a large shift of the transmission spectrum to higher energies for a GT mismatch and a slight shift to lower energy for the AT mismatch. The overall values of the transmission are only weakly changed by the introduction of mismatches. Figure 4(b) shows the ratio of the time-averaged current for the matched sequence to the current with an AC or GT mismatch. The current was calculated at each simulation time step as an integral over the corresponding quantum-mechanical transmission at this time and afterward a time average was performed. In all calculations we have kept the position of the Fermi energy fixed at E_F= −8.0 eV. This value is arbitrary but provides a reference point to cover the spectral range of the transmission functions which are mostly contributing to the current without the need of going to very large biases, where the near-

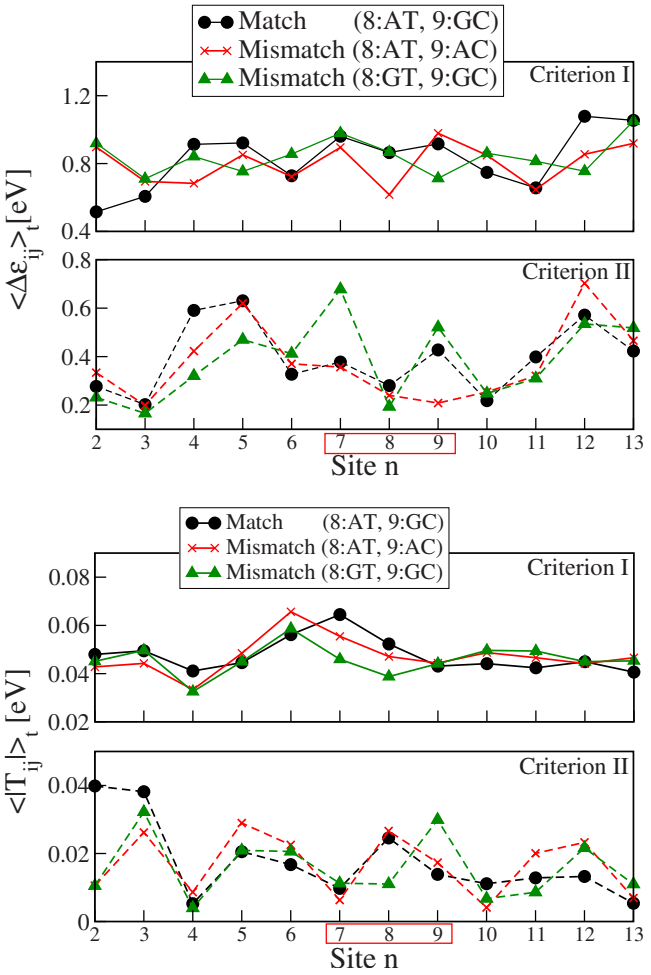

FIG. 5. (Color online) (a) Averaged site-to-site energy gaps and (b) transfer integrals over a 1 ps MD trajectory for criteria I and II.

equilibrium calculations may become questionable. The main feature found here for criterion I is that the current ratio of the matched sequence to the mismatched sequences at low bias can be less than one (especially for GT), indicating that in this approximation there exists a bias range where a mismatched sequence can provide a better pathway for quasicoherent charge transport than a perfect sequence. Obviously, by increasing the bias window this situation may be reversed once the applied bias is large enough to cover lower energy sectors of the transmission spectrum where $\langle T(E,t)\rangle_t$ for the matched sequence becomes larger than for the GT mismatch.

Criterion II yields a different behavior. First of all, the values of the transmission are considerably reduced compared to criterion I since here we are not maximizing the electronic hopping integral alone but finding a compromise between small energy gap and large electronic coupling. As a result, a maximum coupling pathway is not necessarily the dominating one since it may include sites with a large energy gap. This can also be seen in Fig. 5 which shows time-averaged electronic parameters for matched and mismatched sequences. Plotted are $\langle|T_{i,i+1}|\rangle_t$ as well as the energy gap $\langle\Delta\varepsilon_{i,i+1}\rangle_t$ between nearest-neighbor sites. The energy gap barriers are lowered but the average hopping is reduced as well by roughly a factor of 2 for criterion II when comparing with

case I. Figure 5 also clearly demonstrates the effect of GT mismatch. The energy gap for the GT mismatch is considerably increased at site 7($\langle \Delta\varepsilon_{7,8} \rangle_t$). The introduction of this barrier leads to a strong suppression of the transmission for this mismatch. On the contrary, the AC mismatch averaged energy distribution along the chain is not much changed when comparing with the matched case so that the transmission function is not much reduced but only experiences a small shift down to lower energies. The basic effect of these modifications is a dramatic suppression of the current for the GT mismatch (on average by a factor 400) as well as a reduction in the current for the AC mismatch by a smaller factor of order 50.

IV. CONCLUSIONS

An interesting result of the present study has been the demonstration that molecular orbitals of nucleotide fragments are intermittently switching from bases to backbone over the simulation time. However, we also found that the degree of localization onto the backbones can be strongly affected by the theory level used in computing the electronic structure, becoming weaker when using a DFT level instead of a semiempirical AM1 Hamiltonian. A definite conclusion on this issue will require additional studies using, e.g., different base sequences. Hence, the appropriate choice of a fragment as well as the relevant molecular orbitals for coarse graining the electronic structure turns out to be a delicate issue which can have important consequences for the discussion of the charge-transport properties of DNA systems. In relation to this, we further considered two different selection rules for mapping the multilevel electronic structure of the fragments onto a much simpler low-dimensional tight-binding model. The results indicate that a dramatic change in the match to mismatch current ratio, also observed experimentally,[16] could be obtained by choosing the relevant electronic pathway in such a way as to maximize an effective site to site tunneling probability (criterion II). Our methodology could be easily transferred to study charge migration in other systems where dynamical disorder is playing an important role and where the convolution of the orbital space of the full system onto a coarse-grained space becomes more advantageous due to the complexity of the underlying electronic structure. We finally remark that going beyond a description of transport based on the Landauer picture in presence of strong structural fluctuations (time-dependent electronic structure) remains a very challenging issue to be addressed.

ACKNOWLEDGMENTS

The authors acknowledge Giorgia Brancolini, Rosa Di Felice, and Wei-Yuan Tu for very fruitful discussions. S.A. thanks for financial support from the Erasmus Mundus program External Co-operation (EM ECW-L04 TUD 08-11). This work has been supported by the Deutsche Forschungsgemeinschaft (DFG) within the Priority Program 1243 "Quantum transport at the molecular scale" under Contract No. CU 44/5-2, by the Volkswagen Foundation under Grant No. I/78-340, by the European Union under Contract No. IST-029192-2, and the Technology Program ″World Class University″ under Contract No. R31-2008-000-10100-0. We further acknowledge the Center for Information Services and High Performance Computing (ZIH) at the Dresden University of Technology for computational resources.

[1] V. Bhalla, R. P. Bajpai, and L. M. Bharadwaj, EMBO Rep. **4**, 442 (2003).
[2] M. Zwolak and M. Di Ventra, Rev. Mod. Phys. **80**, 141 (2008).
[3] H. W. Ch. Postma, Nano Lett. **10**, 420 (2010).
[4] E. Braun, Y. Eichen, U. Sivan, and G. Ben-Yoseph, Nature (London) **391**, 775 (1998).
[5] P. J. de Pablo, F. Moreno-Herrero, J. Colchero, J. Gómez Herrero, P. Herrero, A. M. Baró, P. Ordejón, J. M. Soler, and E. Artacho, Phys. Rev. Lett. **85**, 4992 (2000).
[6] A. J. Storm, J. van Noort, S. de Vries, and C. Dekker, Appl. Phys. Lett. **79**, 3881 (2001).
[7] Y. Zhang, R. H. Austin, J. Kraeft, E. C. Cox, and N. P. Ong, Phys. Rev. Lett. **89**, 198102 (2002).
[8] D. Porath, A. Bezryadin, S. de Vries, and C. Dekker, Nature (London) **403**, 635 (2000).
[9] H. Cohen, C. Nogues, R. Naaman, and D. Porath, Proc. Natl. Acad. Sci. U.S.A. **102**, 11589 (2005).
[10] B. Xu, P. Zhang, X. Li, and N. Tao, Nano Lett. **4**, 1105 (2004).
[11] N. Kang, A. Erbe, and E. Scheer, Appl. Phys. Lett. **96**, 023701 (2010).
[12] D. Porath, G. Cuniberti, and R. D. Felice, in *Long-Range Charge Transfer in DNA I (II)*, Topics in Current Chemistry Vol. 237, edited by G. B. Schuster (Springer, Berlin, New York, 2004), p. 183.
[13] *Modern Methods for Theoretical Physical Chemistry of Biopolymers*, edited by E. Starikow, S. Tanaka, and J. Lewis (Elsevier, Amsterdam, 2006).
[14] *Charge Migration in DNA: Perspectives from Physics, Chemistry and Biology*, edited by T. Chakraborty (Springer, Berlin, New York, 2007).
[15] K. A. Williams, P. T. M. Veenhuizen, B. G. de la Torre, R. Eritja, and C. Dekker, Nature (London) **420**, 761 (2002).
[16] X. Guo, A. A. Gorodetsky, J. Hone, J. K. Barton, and C. Nuckolls, Nat. Nanotechnol. **3**, 163 (2008).
[17] J. Hihath, B. Xu, P. Zhang, and N. Tao, Proc. Natl. Acad. Sci. U.S.A. **102**, 16979 (2005).
[18] S. O. Kelley, E. M. Boon, J. K. Barton, N. M. Jackson, and M. G. Hill, Nucleic Acids Res. **27**, 4830 (1999).
[19] J. Jortner, M. Bixon, T. Langenbacher, and M. E. Michel-Beyerle, Proc. Natl. Acad. Sci. U.S.A. **95**, 12759 (1998).
[20] F. C. Grozema, S. Tonzani, Y. A. Berlin, G. C. Schatz, L. D. A. Siebbeles, and M. A. Ratner, J. Am. Chem. Soc. **130**, 5157 (2008).
[21] T. Cramer, S. Krapf, and T. Koslowski, J. Phys. Chem. C **111**, 8105 (2007).
[22] A. Troisi and G. Orlandi, J. Phys. Chem. B **106**, 2093 (2002).

[23] R. Gutiérrez, S. Mohapatra, H. Cohen, D. Porath, and G. Cuniberti, Phys. Rev. B **74**, 235105 (2006).
[24] R. Gutiérrez, R. A. Caetano, B. P. Woiczikowski, T. Kubar, M. Elstner, and G. Cuniberti, Phys. Rev. Lett. **102**, 208102 (2009).
[25] P. B. Woiczikowski, T. Kubar, R. Gutierrez, R. Caetano, G. Cuniberti, and M. Elstner, J. Chem. Phys. **130**, 215104 (2009).
[26] R. Gutiérrez, R. Caetano, P. B. Woiczikowski, T. Kubar, M. Elstner, and G. Cuniberti, New J. Phys. **12**, 023022 (2010).
[27] B. B. Schmidt, M. H. Hettler, and G. Schon, Phys. Rev. B **77**, 165337 (2008).
[28] S. Roche, Phys. Rev. Lett. **91**, 108101 (2003).
[29] T. Kubař and M. Elstner, J. Phys. Chem. B **112**, 8788 (2008).
[30] R. N. Barnett, Ch. L. Cleveland, A. Joy, U. Landman, and G. B. Schuster, Science **294**, 567 (2001).
[31] H. Yamada, E. Starikov, and D. Hennig, Eur. Phys. J. B **59**, 185 (2007).
[32] F. C. Grozema, Y. A. Berlin, and L. D. A. Siebbeles, J. Am. Chem. Soc. **122**, 10903 (2000).
[33] C. R. Treadway, M. G. Hill, and J. K. Barton, Chem. Phys. **281**, 409 (2002).
[34] N. J. Turro and J. K. Barton, JBIC, J. Biol. Inorg. Chem. **3**, 201 (1998).
[35] C. Wan, T. Fiebig, S. O. Kelley, C. R. Treadway, and J. K. Barton, Proc. Natl. Acad. Sci. U.S.A. **96**, 6014 (1999).
[36] P. Altoè, M. Stenta, A. Bottoni, and M. Garavelli, Theor. Chem. Acc. **118**, 219 (2007).
[37] H. M. Senn and W. Thiel, Angew. Chem., Int. Ed. **48**, 1198 (2009).
[38] D. A. Case *et al.*, *Amber 10* (University of California, San Francisco, 2008); D. A. Pearlman, D. A. Case, J. W. Caldwell, W. S. Ross, T. E. Cheatham III, S. DeBolt, D. Ferguson, G. Seibel, and P. Kollman, Comput. Phys. Commun. **91**, 1 (1995); D. A. Case, T. Cheatham, T. Darden, H. Gohlke, R. Luo, K. M. Merz, Jr., A. Onufriev, C. Simmerling, B. Wang, and R. J. Woods, J. Comput. Chem. **26**, 1668 (2005).
[39] W. L. Jorgensen and J. D. Madura, J. Am. Chem. Soc. **105**, 1407 (1983).
[40] K. Kitaura and K. Morokuma, Int. J. Quantum Chem. **10**, 325 (1976).
[41] K. Kitaura, E. Ikeo, T. Asada, T. Nakano, and M. Uebayasi, Chem. Phys. Lett. **313**, 701 (1999).
[42] D. G. Fedorov and K. Kitaura, J. Phys. Chem. A **111**, 6904 (2007).
[43] T. Kubař, P. B. Woiczikowski, G. Cuniberti, and M. Elstner, J. Phys. Chem. B **112**, 7937 (2008).
[44] M. J. S. Dewar, E. G. Zoebisch, E. F. Healy, and J. P. Stewart, J. Am. Chem. Soc. **107**, 3902 (1985).
[45] S. Goedecker, M. Teter, and J. Hutter, Phys. Rev. B **54**, 1703 (1996).
[46] http://cp2k.berlios.de/manual/index.html; J. VandeVondele, M. Krack, F. Mohamed, M. Parrinello, T. Chassaing, and J. Hutter, Comput. Phys. Commun. **167**, 103 (2005).
[47] M. Rubio, D. Roca-Sanjuán, M. Merchán, and L. Serrano-Andrés, J. Phys. Chem. B **110**, 10234 (2006).
[48] F. L. Gervasio, P. Carloni, and M. Parrinello, Phys. Rev. Lett. **89**, 108102 (2002).
[49] We have performed electronic-structure calculations on the AM1 level for the two fragments (7:GC and 8:TA) within the matched DNA sequence used in the text. The geometry was optimized using the Amber99 force field in vacuum. The results of our calculations indicate that both HOMO and HOMO-1 levels have a strong weight onto the backbones while base-localized MOs appear at the HOMO-2 level. This is consistent with the results obtained from snapshots along the MD trajectory. Similar calculations were then carried out for deoxythymidine monophosphate anion ($dTMP^-$) optimized in vacuum using again the Amber99 force field. In this case, the HOMO state is localized onto the backbone and a thymine-localized MO appears at the HOMO-4. It seems possible that force-field-optimized geometries and/or the electronic-structure calculation level (AM1) contributed to the discrepancy with the results by M. Rubio *et al.* (Ref. 47), where it came out that the most easily oxidized part of the $dTMP^-$ is the thymine at the CASPT2 level of calculation.
[50] S. S. Mallajosyula, J. C. Lin, D. L. Cox, S. K. Pati, and R. R. P. Singh, Phys. Rev. Lett. **101**, 176805 (2008).